The Astrophysical Journal, 834:89 (9pp), 2017 January 1 doi:10.3847/1538-4357/834/1/89


# NEW EVIDENCE FOR CHARGE-SIGN-DEPENDENT MODULATION DURING THE SOLAR MINIMUM OF 2006 TO 2009

V. Di Felice[1,2], R. Munini[3], E. E. Vos[4], and M. S. Potgieter[4]
[1] INFN, Sezione di Roma "Tor Vergata," I-00133 Rome, Italy
[2] Agenzia Spaziale Italiana (ASI) Science Data Center, Via del Politecnico snc, I-00133 Rome, Italy
[3] INFN, Sezione di Trieste, I-34149 Trieste, Italy
[4] Centre for Space Research, North-West University, 2520 Potchefstroom, South Africa
*Received 2016 July 26; revised 2016 October 21; accepted 2016 October 29; published 2017 January 4*

## ABSTRACT

The PAMELA space experiment, in orbit since 2006, has measured cosmic rays (CRs) through the most recent period of minimum solar activity with the magnetic field polarity as $A < 0$. During this entire time, galactic electrons and protons have been detected down to 70 MV and 400 MV, respectively, and their differential variation in intensity with time has been monitored with unprecedented accuracy. These observations are used to show how differently electrons and protons responded to the quiet modulation conditions that prevailed from 2006 to 2009. It is well known that particle drifts, as one of four major mechanisms for the solar modulation of CRs, cause charge-sign-dependent solar modulation. Periods of minimum solar activity provide optimal conditions in which to study these drift effects. The observed behavior is compared to the solutions of a three-dimensional model for CRs in the heliosphere, including drifts. The numerical results confirm that the difference in the evolution of electron and proton spectra during the last prolonged solar minimum is attributed to a large extent to particle drifts. We therefore present new evidence of charge-sign-dependent solar modulation, with a perspective on its peculiarities for the observed period from 2006 to 2009.

*Key words:* cosmic rays – Sun: activity – Sun: heliosphere – solar wind

## 1. INTRODUCTION

When entering the heliosphere, the charged particles that constitute cosmic rays (CRs) of galactic origin interact with the turbulent solar wind and its embedded heliospheric magnetic field (HMF). They undergo convection, diffusion, and adiabatic energy losses while traversing the expanding solar wind. They also sense the gradients and curvatures in the global HMF, and the effect of the heliospheric current sheet (HCS), causing them to drift according to the polarity of the HMF. The resulting solar modulation significantly modifies the local interstellar CR spectra in intensity and shape, a process that depends on the type of particles, their energy, sign of charge, and solar activity, in terms of both space—i.e., where in the heliosphere they are observed—and time—i.e., when during solar cycles they are measured. CRs with energies up to tens of GeV are affected, progressively more so with decreasing energies, so that below a few GeV their solar modulation becomes considerable; see Strauss & Potgieter (2014b).

At energies above 10 GeV, evidence for CR modulation has been provided for decades by ground-level CR detectors, called neutron monitors. These observations show a clear anticorrelation between the CR intensity and solar activity for the whole 11 year solar cycle, from its minimum, when the Sun is quiet and the CR intensity is at its largest, to its maximum, when the CRs reach their minimum intensity. A 22 year periodicity is also evident in these observations, caused by the polarity reversal of the HMF, which takes place around extreme maximum solar activity, every ~11 years. This 22 year cycle in CRs, which is not at all evident in, e.g., sunspot numbers as a proxy for solar activity, is a manifestation of the effects of particle drifts. In fact, during a polarity cycle of the HMF with $A > 0$[5], when magnetic field lines are pointing outward in the northern heliohemisphere, positively charged particles drift into the inner heliosphere mainly through the polar regions of the heliosphere and then outwards mainly along the wavy HCS. This drift pattern reverses when the HMF changes its polarity, so that during cycles with $A < 0$ positively charged particles reach the Earth mainly through the equatorial regions, directly encountering the wavy HCS in the process. Negatively charged particles then drift inwards mainly through the polar regions. This means that protons and electrons sense different regions of the heliosphere during the same polarity period while travelling through the heliosphere to the Earth, providing a clear signature for charge-sign-dependent modulation; for an elaborate discussion of these effects, see the reviews by Potgieter (2013, 2014a).

Since CRs are responsive to heliospheric modulation conditions, they can be used very effectively to provide fundamental information for our understanding of the features of charged particle transport and also the details of solar modulation, because the interplay between the mentioned major modulation mechanisms varies with solar activity. Moreover, precise CR observations are crucially important when addressing fundamental questions in astrophysics, e.g., particle and antiparticle CR data can be utilised to search for hints of new physics such as dark matter. In addition to the data on high-energy antiparticles (Adriani et al. 2009, 2013a) their low-energy spectra are also interesting since they can be used (e.g., Bottino et al. 2012; Cerdeño et al. 2012; Hooper et al. 2015) to constrain models with light (~10 GeV) dark-matter candidates put forward to interpret measurements by direct-detection experiments (e.g., Aalseth et al. 2011; Belli et al. 2011). However, these data can be fully exploited with a precise understanding of the expected background due to the production of antiparticles by CR interaction with the interstellar matter and their transport to the Earth. Consequently, this requires that the charge-sign-dependent solar

[5] In the complex sun magnetic field, the dipole term nearly always dominates the magnetic field of the solar wind. A is defined as the projection of this dipole on the solar rotation axis.

modulation and how it changes with time are accurately interpreted. The importance of solar modulation is clearly demonstrated by the large variability of CR measurements at energies below a few tens of GeV performed inside the heliosphere by several space and balloon missions over the years, such as the *Voyagers* (Stone et al. 2013), *Ulysses* (Simpson et al. 1992; Heber et al. 2009), and balloon flights (see, e.g., Seo 2012, and references therein).

Since the late 1960s observations made at Earth have been interpreted using modeling of the solar modulation with the force-field approximation (Gleeson & Axford 1968). However, this approach is severely limited in exploring and subsequently explaining the full range of processes responsible for the solar modulation of CRs. The approach is valid for only one spatial dimension, so it cannot account for any process such as diffusion perpendicular to the HMF, or for particle drifts, which essentially require a full 3D approach. The importance of drifts was already illustrated and emphasized in the late 1970s (see Jokipii et al. 1977) and early 1980s with elaborate numerical illustrations by Jokipii & Kota (1985) and Potgieter & Moraal (1985), who also applied their model to charge-sign-dependent observations; see the recent review by Potgieter (2014a). Experimental evidence of charge-sign-dependent solar modulation has gradually built up over the years. Measurements of proton and helium intensities and the sum of electron and positron intensities, performed in the inner heliosphere by balloon-based experiments and spacecraft during cycles of opposite polarity, provided evidence of this effect. Moreover, measurements of positron fraction (Clem & Evenson 2009) clearly show how relevant charge-sign-dependent modulation is below a few GeV. Alongside experimental findings, significant progress has been made in drift theory, supported by increasingly complex and accurate modelling. These models can describe a full 22 year solar cycle (Le Roux & Potgieter 1995) and even predict how drift should change with the solar activity cycle (Ferreira & Potgieter 2004). In addition, the effects of drift on radial and latitudinal gradients have been illustrated (Potgieter et al. 1989; Vos & Potgieter 2016). Comprehensive modeling of the effects of drift was done on the solar modulation of protons, electrons, positrons, and even antiprotons (Webber & Potgieter 1989; Langner & Potgieter 2004; Potgieter & Langner 2004).

In order to improve our understanding of the details of the interplay among the several mechanisms for solar modulation, in particular the importance of drifts during solar minimum epochs and over the entire solar cycle, precise and simultaneous measurements are required of CRs with opposite charge signs. Nowadays, such precise measurements are being performed in space by the magnetic spectrometers PAMELA (Adriani et al. 2014), a satellite-borne experiment, and AMS-02 (Aguilar et al. 2014, 2015), on board the *International Space Station*. Fortunately, the PAMELA experiment has obtained data during the entire peculiar and extraordinarily prolonged solar minimum with $A < 0$ of cycle 23/24, which lasted until the end of 2009 (Potgieter 2013, and references therein). This mission has been detecting CR spectra for protons, electrons, and positrons from a few tens of MeV to several hundreds of GeV. A report of how the $e^+/e^-$ ratios between 0.5 and 5.0 GeV changed from 2006 to 2015 has recently been produced (Adriani et al. 2016). Here, we show the temporal evolution of electron and proton spectra during the last solar minimum, in conjunction with comprehensive modelling, exploring and utilizing the extended energy range and improved precision. These differences will be displayed respectively as proton and electron time profiles, from 2006 to 2009, together with the $e^-/p$ ratio as a function of rigidity for this period. Evidently, with the observation of precise spectra for protons, electrons, positrons, and even antiprotons, on an almost continuous timescale, charge-sign-dependent modulation, and other important 3D effects, should no longer be ignored when interpreting these data, so that surpassing the force-field model has become necessary; see also Maccione (2013) and Cholis et al. (2016).

## 2. THE PAMELA ELECTRON AND PROTON DIFFERENTIAL FLUXES

The PAMELA spectrometer was conceived and built to study the antimatter component of CRs over a wide energy range, from tens of MeV up to hundreds of GeV, significantly improving collected statistics and precision with respect to previous experiments. The magnetic spectrometer, composed of a permanent magnet and a tracking system of six planes of double-sided silicon sensors, reconstructs the particle trajectory and determines its curvature, distinguishing oppositely charged particles; it also provides a measure of the particle rigidity $R = pc/Ze$ ($p$ and $Ze$ being the particle momentum and charge, respectively, and $c$ the speed of light) and of ionization energy losses. The particle velocity is obtained combining the information on time of passage given by the time-of-flight system with the track length. With this information the spectrometer can distinguish between downward-going particles and upward-going splash-albedo particles, and can separate negatively from positively charged particles. Hadron–lepton separation is achieved thanks to a sampling imaging calorimeter. A shower tail catcher and a neutron detector beneath help in the discrimination, while an anticoincidence system is used to reject spurious events. More details on the instrument can be found in Picozza et al. (2007).

Such apparatus is optimized for the study of singly charged particles and to reach a high level of electron–proton discrimination. Thus, aside from antimatter studies, PAMELA also performed precise measurements of the matter component of CRs (Adriani et al. 2014). In particular, galactic electron and proton differential fluxes have been measured up to ~600 GV and ~1 TV respectively (Adriani et al. 2011a, 2011b), and down to energies as low as a few tens of MeV. Since its launch in 2006 June, the instrument has followed a quasi-polar orbit at an inclination of 70°, sampling regions of low geomagnetic cutoff at high latitude. Thus, the lowest detectable rigidity limit is not due to the effects of geomagnetic cutoff, but to the high curvature of low-energy particles in the instrument's magnetic field, which causes them not to trigger.

The long-duration flight allowed the collection of data during the entire solar minimum of 2006–2009 with $A < 0$, and continuous monitoring of the flux of charged particles of galactic origin. Adriani et al. (2013b) reported time-dependent measurements of the proton flux, performed by PAMELA down to 400 MV, which are relevant for studies of solar modulation and are used in this work. The large statistics collected allowed the average proton flux to be measured over each Carrington rotation (Carrington 1863), from number 2045 to 2092 (hereafter referred as Carrington flux). We also use data on galactic electron flux measured by PAMELA during the same period, as reported by Adriani et al. (2015). Due to the lower statistics the $e^-$ fluxes were measured over a six-month time basis. PAMELA data are

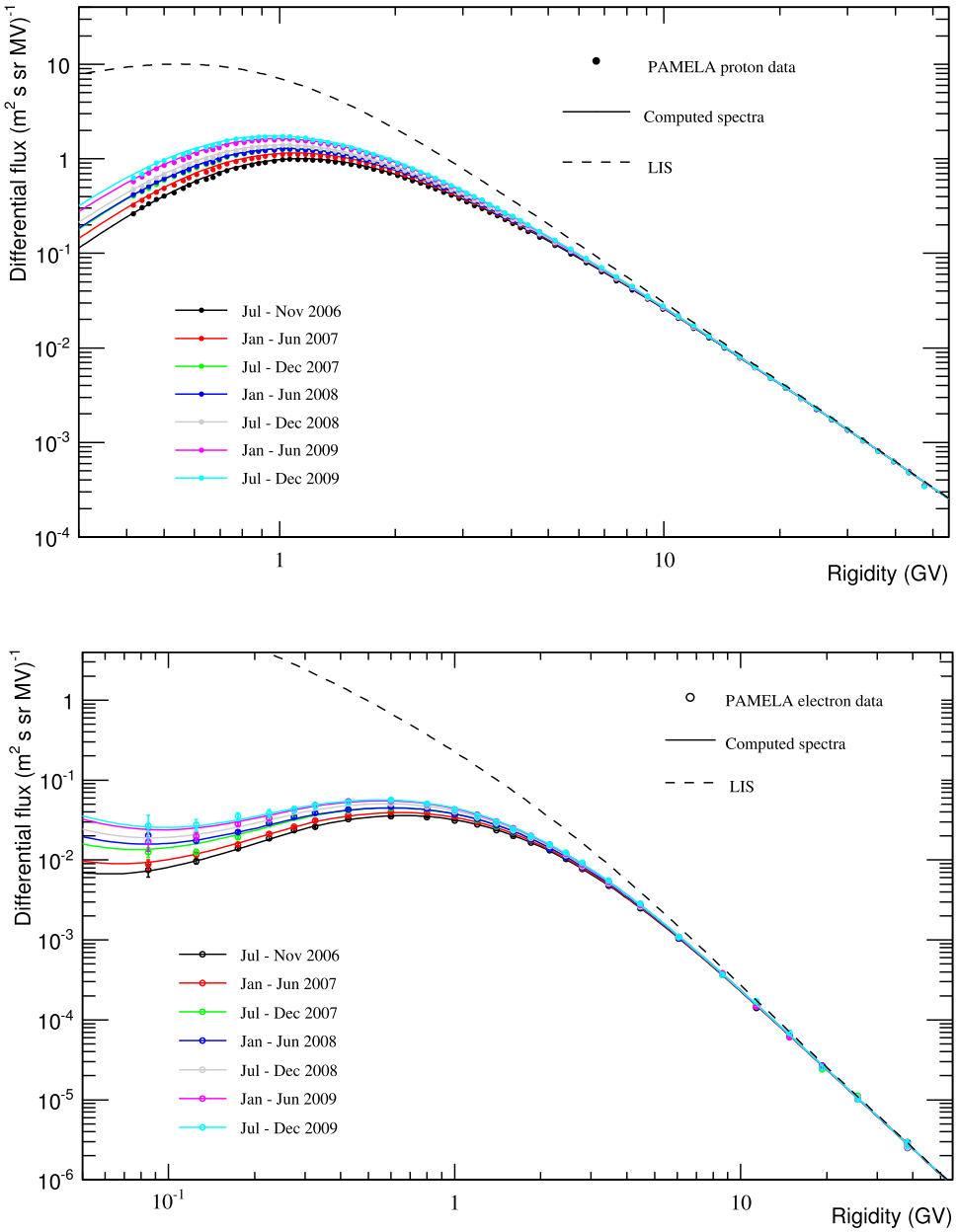


**Figure 1.** Proton (upper panel) and electron (lower panel) spectra averaged over six months as measured by PAMELA from mid-2006 to the end of 2009 (Adriani et al. 2013b, 2015) are shown as a function of the rigidity. Observations are overlaid with the corresponding computed spectra (continuous lines) for magnetic field polarity in a cycle with $A < 0$ (Potgieter et al. 2014b, 2015; Vos & Potgieter 2015). Color coding shown in the legend indicates the seven selected time slots for both experimental and computed spectra. The proton and electron LIS (dashed lines) used for the computation are also shown.

obtained through the Cosmic Ray Data Base of the ASI Science Data Center (ASDC Cosmic Ray Database[6]).

In order to compare the spectral evolution of protons and electrons, proton data have been combined on a semestral time basis, conforming to the temporal division of the electron measurements. For each semester a galactic proton differential flux, $\varphi$, has been obtained by performing a weighted average of the relevant Carrington fluxes, $\varphi_i$:

$$\varphi = \frac{\sum_{i=1}^{N} \varphi_i w_i}{\sum_{i=1}^{N} w_i} \quad (1)$$

where $i$ is the index running on the number $N$ of Carrington rotations within the considered semester, and the weight $w_i$ is the number of active days of the instrument for the $i$th Carrington rotation. This procedure resulted in seven differential proton fluxes as a function of kinetic energy for each semester from 2006 July to 2009 December.

For a quantitative understanding of the different temporal development of the electron and proton spectra it is necessary to compare their recovery to solar minimum at the same rigidities. Particle spectra available as fluxes in kinetic energy, $\varphi(E)$, in units of (m$^2$ s sr MeV)$^{-1}$, have been converted to fluxes in rigidity, $\varphi(R)$, in units of (m$^2$ s sr MV)$^{-1}$, according to the following:

$$\varphi(R) = \varphi(E) \frac{R}{\sqrt{R^2 + m^2}} \quad (2)$$

[6] ASDC Cosmic Ray Database. n.d., http://tools.asdc.asi.it/cosmicRays.jsp.

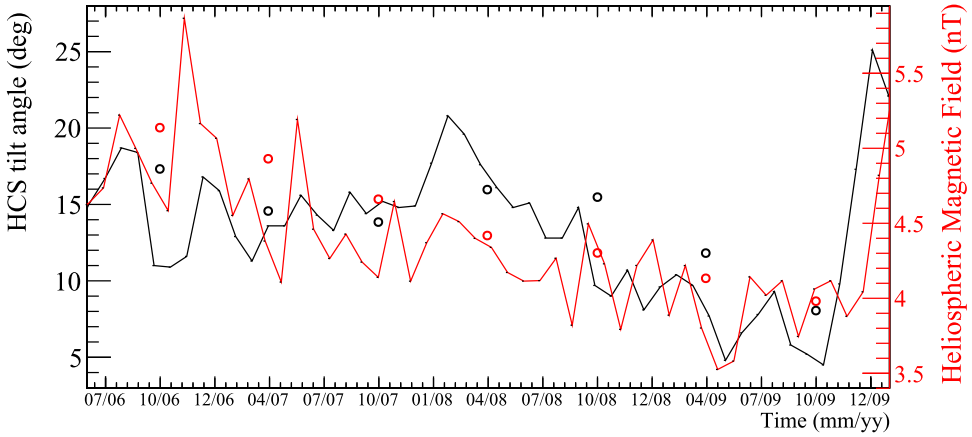


**Figure 2.** Temporal evolution of the HCS tilt angle (black line) and the HMF (red line) from mid-2006 to the end of 2009. Data are taken from Wilcox Solar Observatory (Wilcox Solar Observatory. n.d., http://wso.stanford.edu/) and ACE data (ACE data. n.d., http://omniweb.gsfc.nasa.gov/), respectively. The open points represent the average values for the preceding 12 months, used as input for the modeling to compute the seven averaged electron and proton spectra. See also Vos & Potgieter (2015).

with $m$ the particle mass. The application of Equation (2) in the energy range of the PAMELA measurement results in a significant modification of the proton spectral shape below a few tens of GeV, while the effect on the electron flux is negligible due to their lower mass. The resulting proton and electron spectra as a function of rigidity are shown in Figure 1. Error bars represent the statistical errors. Because of statistical requirements, electrons and protons were measured in different rigidity intervals in the whole range of interest, and this will be detailed in Section 4 when comparing the temporal evolution of particle intensities over the whole rigidity range. Solid lines in these figures are the solutions of a comprehensive numerical modulation model, reproducing the particle differential spectra for each period as indicated. For both electrons and protons the newly determined local interstellar spectra (LIS, see also Potgieter et al. 2014a) used as unmodulated input spectra for the model are also shown in the two figures.

The different behavior of electrons in comparison with protons at low rigidities was discussed in detail by Potgieter et al. (2014b, 2015) and is not repeated here. In the rest of our work, we focus on rigidities above 0.4 GV, which is the lowest rigidity available for the proton spectra. Relevant aspects of the theory and modeling are concisely described in Section 3 of this paper. For both CR species, the low-energy part of the spectrum varies significantly with time, responding to changes in solar activity during the observed solar minimum period. As expected, the lowest energies are the most responsive.

## 3. MODULATION THEORY AND NUMERICAL MODELING

A comprehensive 3D numerical model was implemented to study the changing proton and electron fluxes measured by PAMELA during the solar minimum of cycle 23/24, following similar studies by Potgieter et al. (2014b, 2015). The model used in this study is based on the transport equation of Parker (1965), which describes the transport and modulation of CRs in the heliosphere. The advantage of this model over traditional models based on a force field is that all of the important modulation processes are explicitly accounted for, namely diffusion in all dimensions, convection, adiabatic energy losses, and drifts, which allows for an in-depth study of heliospheric modulation. See Potgieter (2013) for a detailed overview of heliospheric modulation and the various modulation processes.

Using the above model, energy spectra were computed that reproduce PAMELA proton and electron measurements, as shown in Figure 1. The heliopause (HP) for the simulated heliosphere was taken at 122 au, with a position of the termination shock that varies between 88 au in 2006, and 80 au in 2009. LIS are specified for protons and electrons at the HP, as reported in other works (Potgieter 2014b; Potgieter et al. 2014a, 2015; Vos & Potgieter 2015), and serve as input spectra at this modulation boundary. Both the electron and proton LIS were constructed to match *Voyager 1* measurements below 100 MeV, taken from beyond the HP in 2012 August, and PAMELA measurements above ~30 GeV, where measurements are expected to become less affected by solar modulation (e.g., Strauss & Potgieter 2014a). This approach leads to reliable estimates for both the proton and electron LIS (see also Potgieter et al. 2015; Vos & Potgieter 2015).

The HCS tilt angle, also seen as a proxy for solar activity, and the magnitude of the HMF at the Earth changed during the years leading up to 2009. Both are important entities for describing drift modulation. When reproducing the PAMELA proton and electron spectra these changes were accounted for by setting up realistic modulation conditions in the model that coincide with the semesterly averaged spectra from PAMELA. Averages for the HCS tilt angle and the HMF were calculated in order to obtain representative values for these parameters that are indicative of preceding modulation conditions. Both the HCS tilt angle and the HMF used in the model are shown in Figure 2. The HMF became more ordered over the years leading up to 2009, which translates to a reduction in the amount of turbulence in the heliosphere and to subsequent increases in the particle mean free paths (MFPs). These increases, along with drifts in gradient, curvature, and current sheet, are expected to be responsible for the increases in proton and electron intensities observed by PAMELA from 2006 to 2009. In this study the HMF is described according to Smith & Bieber (1991); for details see also Vos (2016).

The numerical solutions (lines) shown in Figure 1 were obtained using a diffusion approach that approximates quasi-linear theory, while still adhering to constraints from more advanced turbulence studies (e.g., Potgieter 2000;

Shalchi 2009). The equation for diffusion parallel to the average background HMF is given by

$$\kappa_{\parallel} = \kappa_{\parallel 0}\beta\, F(r, \theta, \phi)\, G(R), \quad (3)$$

with $\kappa_{\parallel 0}$ a constant in units of $cm^2\ s^{-1}$ and $\beta$ the ratio of particle speed to the speed of light. $F(r, \theta, \phi)$ is a function that provides a $B^{-1}$ spatial dependence for the diffusion coefficients, with $B$ the magnitude of the HMF at a given position in the heliosphere, and $r$, $\theta$, and $\phi$ the radial distance, polar angle, and azimuthal angle, respectively. $G(R)$ is a function that takes care of the rigidity dependence, which consists of two combined power laws. For diffusion perpendicular to the HMF lines, a distinction is made between the radial ($\kappa_{\perp r}$) and polar ($\kappa_{\perp \theta}$) directions, where the former and latter are scaled to 2% and 1% of $\kappa_{\parallel}$, respectively. See Vos & Potgieter (2015) for detailed discussions on this approach to diffusion.

Of particular importance to this study is particle drifts, which are caused by the presence of gradients and curvatures in the HMF, as well as by the sudden change in HMF polarity across the HCS. In the weak-scattering limit, which translates to the largest possible drift effects from drift theory, the expression for the average drift velocity of the guiding center is given by

$$\langle \boldsymbol{v_D} \rangle = \nabla \times \kappa_D \boldsymbol{e_B}, \quad (4)$$

with $\boldsymbol{e_B} = \boldsymbol{B}/B$ a unit vector directed along the HMF vector $\boldsymbol{B}$, and $\kappa_D$ a generalized drift coefficient that is related to the drift scale ($\lambda_D$) and the particle speed ($v$) by $\lambda_D = 3\kappa_D/v$. The weak-scattering approach was found to be too simple for the purpose of this study, so a modification had to be applied to $\kappa_D$ that takes into account the effects of scattering on drifts, leading to smaller drift scales at lower rigidities (e.g., Burger et al. 2000). The drift coefficient is therefore given by

$$\kappa_D = \kappa_{D0}\,\frac{\beta R}{3B}\,\frac{\left(\frac{R}{R_{D0}}\right)^2}{1+\left(\frac{R}{R_{D0}}\right)^2}, \quad (5)$$

with $\kappa_{D0}$ a constant that determines the amount of drift (taken here as 1.0 for 100% drift effects), and $R_{D0} = 0.55$ GV a constant in GV that determines the rigidity below which $\kappa_D$ is modified. Deviating from the weak-scattering approach to drift prevents the overestimation of drift effects, even under perfect solar minimum conditions, as were present during 2009. This approach of reducing drifts at lower rigidities was originally introduced to explain the very small latitudinal CR gradients observed by *Ulysses* (Heber et al. 2002, 2008; Heber & Potgieter 2006). In the work presented here, this particular reduction in terms of rigidity above 0.4 GV is less important.

Figure 3 shows the rigidity dependence of the MFPs and drift scales for the second semesters of each year of protons and electrons, for 2006 (red) and 2009 (blue), as obtained from the reproduction of PAMELA spectra above 0.4 GV. Parallel MFPs ($\lambda_{\parallel}$) are shown by the solid lines, while perpendicular MFPs in the radial ($\lambda_{\perp r}$) and polar ($\lambda_{\perp \theta}$) directions are given by the dashed and dashed–dotted lines, respectively. The drift scales are given by the dotted lines. From 2006 to 2009, proton and electron MFPs increased by almost the same values above about 2 GeV as solar modulation conditions became quieter (see Potgieter et al. 2014b, 2015; Vos & Potgieter 2015, 2016; Vos 2016). Below 2 GeV this time-dependent increase is somewhat larger for protons than electrons. As required by turbulence theory (e.g., Burger et al. 2000), proton MFPs have a stronger rigidity dependence above ~4 GV than below it. The electron MFPs show this change in rigidity dependence only below about 0.45 GV. Below this rigidity, the electron MFPs become independent of rigidity as discussed by Potgieter et al. (2015). For this study, this feature is less relevant, although important for the total modulation of electrons, as is evident in Figure 1. See also Potgieter & Nndanganeni (2013).

Using a similar numerical model, Nndanganeni & Potgieter (2016) calculated the effect of drifts on the electron propagation by taking the ratio of spectra with $A > 0$ to spectra with $A < 0$, for the same solar activity conditions. Figure 4 shows similar ratios for proton (left panel) and electron (right panel) spectra calculated in this work for the second semester of 2006 (red lines) and 2009 (blue lines). These are computed by assuming that the same quiet modulation conditions will occur during the next solar minimum (cycle with $A > 0$) as during the solar minimum (cycle with $A < 0$) of 2006–2009. In this figure any deviation of this ratio from unity is indicative of drift effects. It follows from these figures that drift effects for electrons are already significant above 0.4 GV, and subside gradually to become less significant above a few GV; for protons this is also the case, but notice that drifts cause proton intensities to be higher in the cycle with $A > 0$ than in the cycle with $A < 0$ for most of the considered rigidities. For electrons, on the other hand, the intensities with $A > 0$ are less than for the cycle with $A < 0$. These results thus illustrate the extent of drift effects when solar minimum conditions are present, as was the case from 2006 to 2009. It follows that drift effects already become significant from a few tens of MV to a few GV. Experimental validations of this numerical model are essential both to determine the rigidity dependence of the modulation parameters and to explore the rigidity range of drifts inside the heliosphere.

The experimental evidence that we present here consists of showing how the proton intensities evolved with time compared to the electron intensities for 2006–2009 and how the differences subside with increasing rigidity compared to what the model indicates.

## 4. DISCUSSION

As mentioned in Section 1, prior to PAMELA observations there was experimental evidence of charge-sign-dependent solar modulation effects being present. In particular, the *Ulysses* mission provided the opportunity to study the long-term propagation and modulation of galactic CRs through measurements of electrons (sum of $e^-$ and $e^+$), protons, and helium in specific energy channels below a few GeV (Heber et al. 2002, 2009). This mission, launched on 1990 October 6, followed a highly inclined (80°.2) elliptical orbit around the Sun until the switch-off in 2009 June, and was the only spacecraft exploring high-latitude regions of the inner heliosphere. The variation in intensity observed along its orbit was reproduced by the modulation modeling from Ferreira & Potgieter (2004), including all the main physical transport processes in the heliosphere. The measured variation of the e/p ratio, especially its latitudinal variation, was interpreted in terms of both temporal and spatial effects, indicating that drift effects are important over a large part of the 11 year solar cycle. Ferreira & Potgieter (2004) also emphasized the importance of simultaneous measurements of protons and electrons in order to

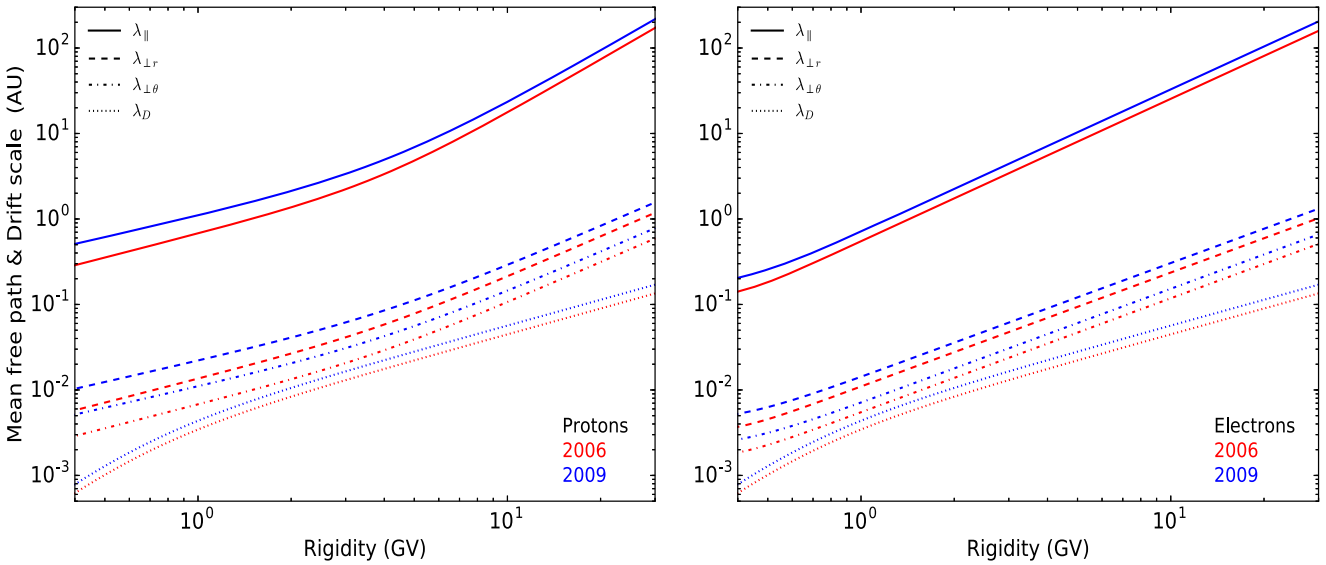


**Figure 3.** Left panel: the mean free paths (MFPs) and drift scales for the diffusion and drift coefficients, as used in modeling the proton modulation, are shown for the second semesters of 2006 (red) and 2009 (blue). Parallel MFPs are given by the solid lines, while perpendicular diffusion in the radial and polar directions is given by the dashed and dashed–dotted lines. The drift scale is shown by the dotted lines. Right panel: similar to left panel, but for electrons.

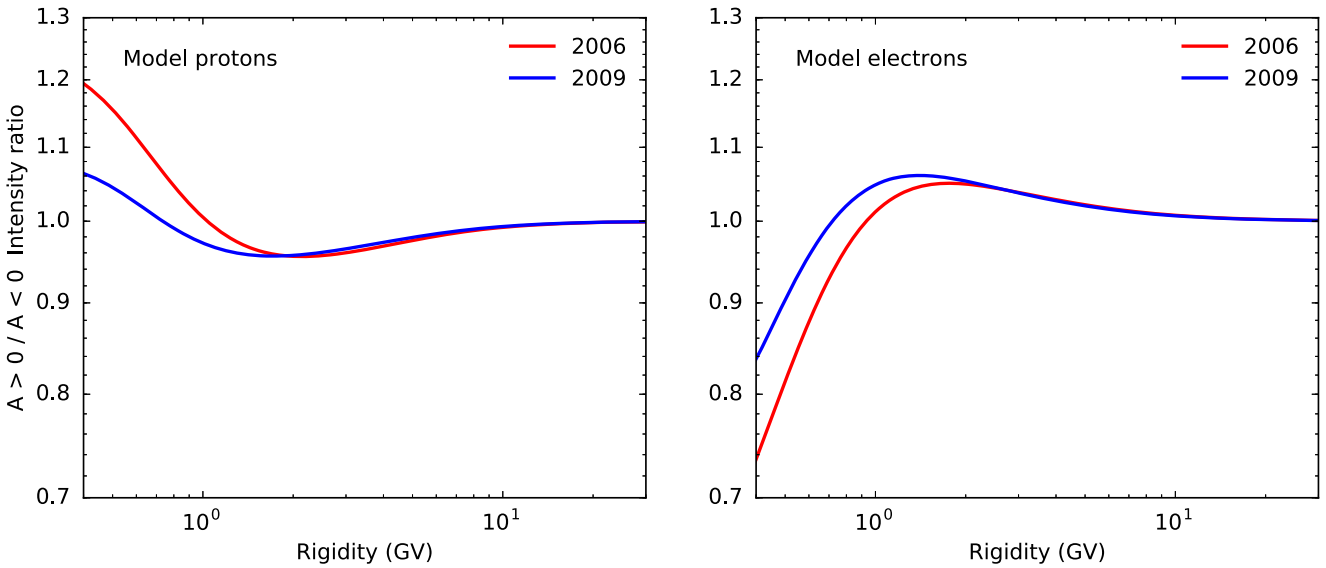


**Figure 4.** Computed ratios of proton (left panel) and electron (right panel) spectra with $A > 0$ and $A < 0$ at the Earth (1 au), for the second semester of 2006 (red lines) and 2009 (blue lines). These ratios are indicative of how large drift effects are in terms of rigidity.

understand and appreciate drift effects. See also the review by Heber & Potgieter (2006).

The PAMELA low-energy data discussed in Section 2 extend the study of the temporal evolution of electron ($e^-$) and proton intensities over a much wider rigidity range than before. Figure 5 illustrates how the proton and electron intensities changed with time from the second half of 2006 to the end of 2009, for several selected rigidity intervals. In order to compare the fluxes at the same rigidities, we use the electron rigidity as a reference and select the corresponding proton intensity by performing a linear interpolation of the measured proton spectrum. Each panel refers to a different rigidity interval, increasing from top to bottom and from left to right. Intensities are normalized to the values measured between 2006 July and 2006 November. The error bars are the quadratic sum of the statistical and systematic uncertainties. The results shown in this figure emphasize that electron and proton intensities developed differently over the last solar minimum period, showing a significantly steeper recovery trend toward solar minimum modulation for protons than for electrons in response to solar modulation conditions. Additionally, the figure shows how these differences dissipate with increasing rigidity. The top left panel presents the measurement at the lowest rigidity available for comparison, between 0.35 and 0.5 GV. In this rigidity range protons increased by a factor of ∼2.4 over about three years, while electrons increased by only a factor of ∼1.6 over the same period.

Comparing the data with the model results shows that the model is able to reproduce the increase in proton and electron intensity observed by PAMELA from 2006 to 2009, in particular the larger relative increase for protons than for electrons, which is indicative of drifts. Figure 6 compares PAMELA proton (upper left) and electron (lower left) measurements with computed proton (upper right) and electron

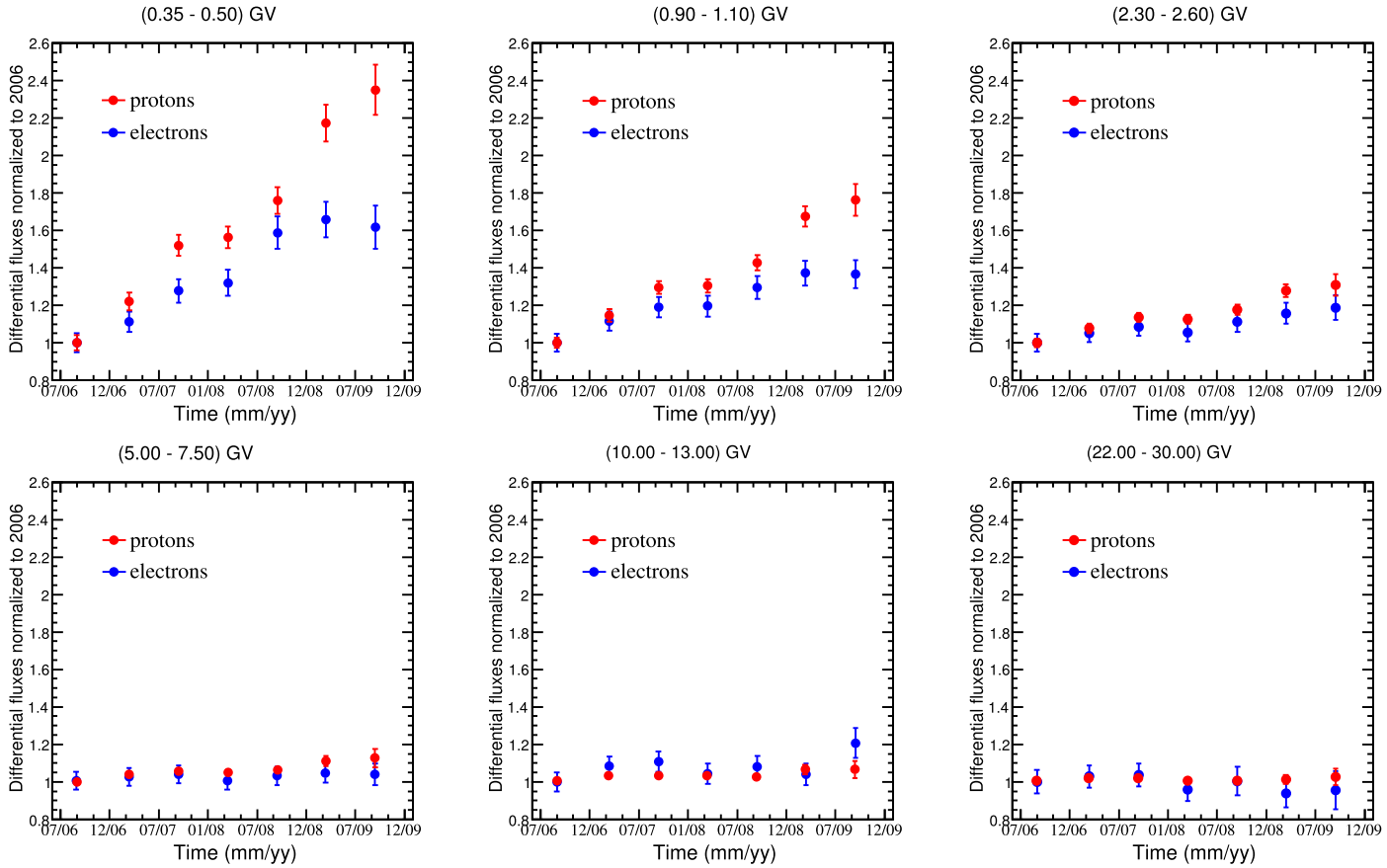


**Figure 5.** Normalized electron and proton intensities, measured from 2006 July to 2009 December for a selection of six rigidity intervals, increasing from left to right and from top to bottom as indicated. The intensity–time profiles are normalized with respect to the averaged intensity measured from 2006 July to November.

(lower right) intensities from the model, at the same rigidities. Similarly to Figure 5, PAMELA and model intensities are shown as a function of time, normalized to the last semester of 2006. It is worth noting that a comprehensive 3D modulation model, which includes drifts resulting in effects due to charge-sign modulation, is able to account for the experimental data. The differences reported in Figures 5 and 6 are interpreted as an indication of particle drifts: the protons mainly drift in along the equatorial regions of the heliosphere, encountering and following the wavy HCS. When the waviness slowly subsides with less solar activity, the tilt angle follows and is reduced, making the modulation conditions more favorable for protons to reach the Earth; their intensity then increases faster than that of electrons, which mostly drift inwards through the polar regions of the heliosphere and thus mostly escape the changes in the waviness of the HCS. During this time, the electrons reach their maximum intensity levels sooner than the protons, and level off already by the end of 2008, whereas the proton intensity keeps increasing as the tilt angle keeps decreasing.

Figure 5 shows that with increasing rigidity (from top to bottom, left to right), this difference in the behavior of protons and electrons gradually diminishes, becoming less pronounced and eventually seeming to subside completely above ∼11 GV. This observed phenomenon is interpreted as an indication of how drift effects subside with increasing rigidity while solar activity decreases. This seems to be in contradiction with Equation (5), according to which the drift coefficient scales in proportion to rigidity at larger rigidities. However, whereas the drift coefficient and the corresponding CR drift velocity in Equation (4) increase, the other modulation processes reduce the global intensity gradients between the LIS value and the intensity at the Earth with decreasing solar activity, so that drift effects effectively diminish. This subtle modulation effect is described in detail by Nndanganeni & Potgieter (2016). PAMELA observations indicate that during the solar minimum period from 2006 to 2009, drift effects were not observable beyond about 10–13 GV.

Figure 7 shows the rigidity dependence of the $e^-/p$ ratios for the spectra measured by PAMELA (symbols) and computed spectra (solid lines) for each semester, from 2006 July to 2009 December, illustrating the observed differences between the two oppositely charged CRs. At lower rigidities a decreasing trend in the $e^-/p$ ratio is observable as the heliospheric conditions change. The dashed line represents the $e^-/p$ ratio based on the respective LIS. The ratios given by the computed spectra give a good representation of the observed PAMELA $e^-/p$ ratios with regard to shape and values over the studied rigidity range. The level of agreement between modeling results and experimental data is shown in the lower panel for two selected time periods in terms of ratio of data to model. Evidently, as solar modulation gets less with increasing rigidity, the $e^-/p$ ratio approaches the LIS ratio. These ratios show that charge-sign modulation is largest in the lowest rigidity interval observed (350–500 MV), in agreement with the model. However, the models suggest that drift effects should reach a maximum around 100 MV for both electrons and protons (Nndanganeni & Potgieter 2016).

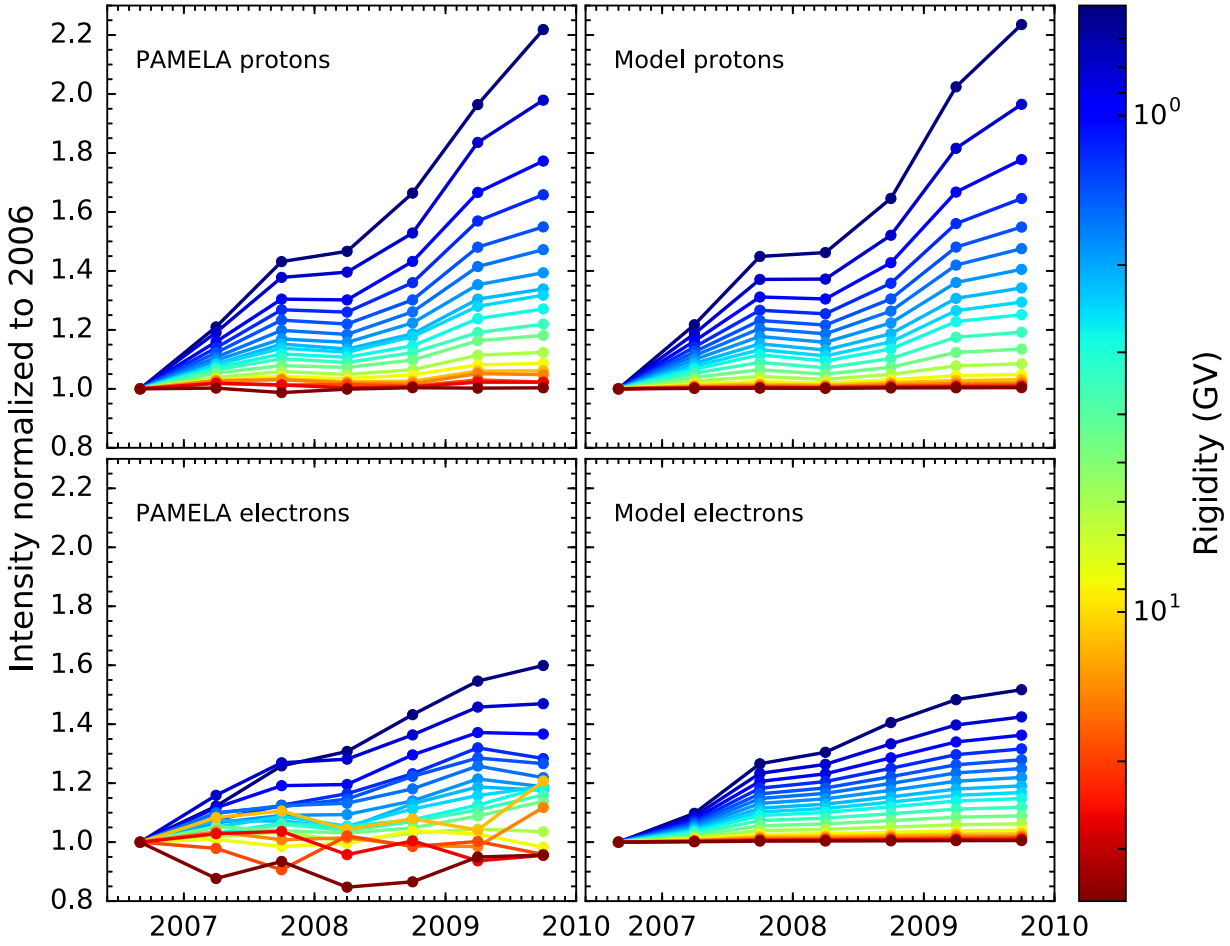


**Figure 6.** Comparison of differential intensity measurements from PAMELA (left panels) and computed intensities from the model (right panels) for protons (top panels) and electrons (bottom panels). Intensities are shown as a function of time, normalized to the second semester of 2006. Rigidity values are indicated by the different colors, according to the colorbar, with high rigidities (around 30 GV) represented by the red lines and low rigidities (around 1 GV) by the blue lines.

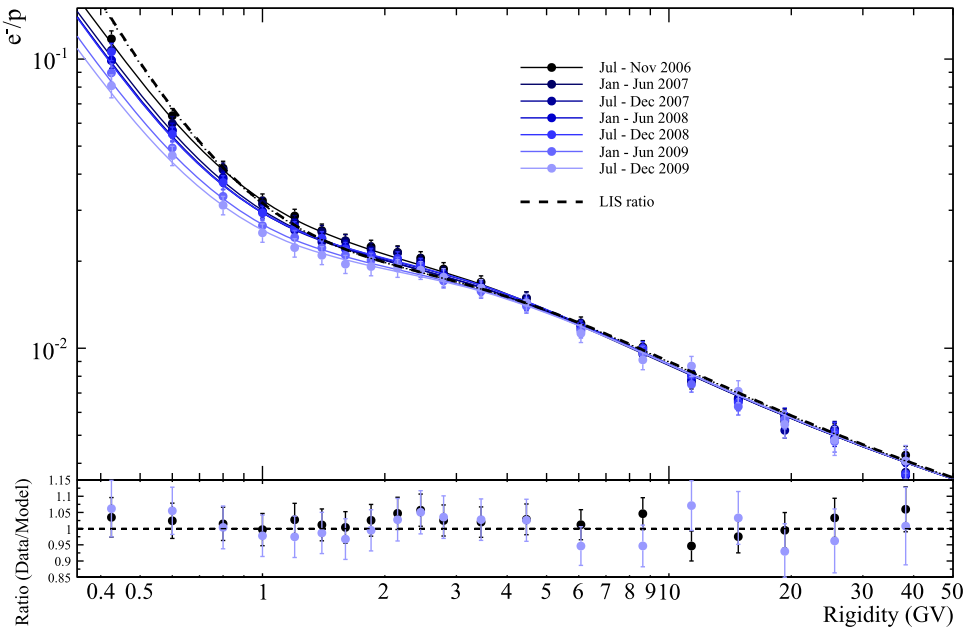


**Figure 7.** Top panel: ratio of electrons to protons measured by PAMELA from 2006 to 2009 indicated by data points with error bars. Solid lines represent the modeling results for the same periods, while the dashed line is the LIS ratio of electrons to protons. Bottom panel: ratio of data to model for 2006 and the second semester of 2009. The ratios show that the model reproduces the experimental data within the experimental errors.

## 5. SUMMARY AND CONCLUSIONS

Simultaneous observations of oppositely charged CRs have been made available by the PAMELA space spectrometer, which measured particle spectra during the entire minimum of solar cycle 23/24 with polarity $A < 0$. We compared proton and electron spectra measured by PAMELA for rigidities between 400 MV and 50 GV. Data show that, as solar activity gradually decreased from 2006 to 2009, low-energy protons presented a different behavior to electrons over time, with proton intensities responding more to changing heliospheric conditions at the same rigidities. We studied the evolution of the spectra for both particles with a comprehensive 3D modulation model, which accounted for all the important modulation processes, including drift. We conclude that the observed effect, subsiding with increasing rigidity, can only be fully accounted for by including drifts, providing new and additional evidence of charge-sign-dependent solar modulation during a period of very quiet solar activity.

This work was supported by INFN and ASI under ASI-INFN Agreement No.2014-037-R.0. M.S.P. and E.E.V. acknowledge partial financial support from the the South African National Research Foundation (NRF) under their Research Cooperation Programme. E.E.V. thanks the Space Science Division of the South African Space Agency (SANSA) for partial financial support during his PhD studies. R.M. acknowledges partial financial support from The Italian Space Agency (ASI) under the program "Programma PAMELA—attivita" scientifica di analisi dati in fase E." The authors would like to thank Dr. M. Boezio for the useful discussion and helpful suggestions. Part of this work is based on archival data provided by the ASI Science Data Center (ASDC).

## REFERENCES

Aalseth, C. E., Barbeau, P. S., Bowden, N. S., et al. 2011, PhRvL, 106, 131301
Adriani, O., Barbarino, G. C., Bazilevskaya, G. A., et al. 2009, Natur, 458, 607
Adriani, O., Barbarino, G. C., Bazilevskaya, G. A., et al. 2011a, PhRvL, 106, 201101
Adriani, O., Barbarino, G. C., Bazilevskaya, G. A., et al. 2011b, Sci, 332, 69
Adriani, O., Barbarino, G. C., Bazilevskaya, G. A., et al. 2013a, PhRvL, 111, 081102
Adriani, O., Barbarino, G. C., Bazilevskaya, G. A., et al. 2013b, ApJ, 765, 91
Adriani, O., Barbarino, G. C., Bazilevskaya, G. A., et al. 2014, PhR, 544, 323
Adriani, O., Barbarino, G. C., Bazilevskaya, G. A., et al. 2015, ApJ, 810, 142
Adriani, O., Barbarino, G. C., Bazilevskaya, G. A., et al. 2016, PhRvL, 116, 241105
Aguilar, M., Aisa, D., Alpat, B., et al. 2015, PhRvL, 114, 171103
Aguilar, M., Aisa, D., Alvino, A., et al. 2014, PhRvL, 113, 121102
Belli, P., Bernabei, R., Bottino, A., et al. 2011, PhRvD, 84, 055014
Bottino, A., Fornengo, N., & Scopel, S. 2012, PhRvD, 85, 095013
Burger, R. A., Potgieter, M. S., & Heber, B. 2000, JGR, 105, 27447
Carrington, R. C. 1863, Made at Redhill (London: Williams and Norgate)
Cerdeño, D. G., Delahaye, T., & Lavalle, J. 2012, NuPhB, 854, 738
Cholis, I., Hooper, D., & Linden, T. 2016, PhRvD, 93, 043016
Clem, J., & Evenson, P. 2009, JGR, 114, A10108
Ferreira, S. E. S., & Potgieter, M. S. 2004, ApJ, 603, 744
Gleeson, L. J., & Axford, W. I. 1968, ApJ, 154, 1011
Heber, B., Gieseler, J., Dunzlaff, P., et al. 2008, ApJ, 689, 1443
Heber, B., Kopp, A., Gieseler, J., et al. 2009, ApJ, 699, 1956
Heber, B., & Potgieter, M. S. 2006, SSRv, 127, 117
Heber, B., Wibberenz, G., Potgieter, M. S., et al. 2002, JGRA, 107, 1274
Hooper, D., Linden, T., & Mertsch, P. 2015, JCAP, 2015, 021
Jokipii, J. R., & Kota, J. 1985, in Proc. ICRC, Vol. 4, Spatial variation of cosmic rays near the heliospheric current sheet (Hampton, VA: STI), 449
Jokipii, J. R., Levy, E. H., & Hubbard, W. B. 1977, ApJ, 213, 861
Langner, U. W., & Potgieter, M. S. 2004, JGRA, 109, a01103
Le Roux, J. A., & Potgieter, M. S. 1995, ApJ, 442, 847
Maccione, L. 2013, PhRvL, 110, 081101
Nndanganeni, R. R., & Potgieter, M. S. 2016, AdSpR, 58, 453
Parker, E. N. 1965, P&SS, 30, 9
Picozza, P., Galper, A., Castellini, G., et al. 2007, APh, 27, 296
Potgieter, M. 2013, LRSP, 10, 3
Potgieter, M. 2014a, AdSpR, 53, 1415
Potgieter, M. 2014b, BrJPh, 44, 581
Potgieter, M. S. 2000, JGR, 105, 18295
Potgieter, M. S. 2013, LRSP, 10, 3
Potgieter, M. S., & Langner, U. W. 2004, ApJ, 602, 993
Potgieter, M. S., Le Roux, J. A., & Burger, R. A. 1989, JGRA, 94, 2323
Potgieter, M. S., & Moraal, H. 1985, ApJ, 294, 425
Potgieter, M. S., & Nndanganeni, R. R. 2013, Ap&SS, 345, 33
Potgieter, M. S., Vos, E., & Nndanganeni, R. 2014a, in Proc. 14th ICATPP Conf., Astroparticle, Particle, Space Physics and Detectors for Physics Applications, ed. S. Giani et al. (Singapore: World Scientific), 204
Potgieter, M. S., Vos, E. E., Boezio, M., et al. 2014b, SoPh, 289, 391
Potgieter, M. S., Vos, E. E., Munini, R., Boezio, M., & Di Felice, V. 2015, ApJ, 810, 141
Seo, E. 2012, APh, 39-40, 76
Shalchi, A. 2009, in Astrophysics and Space Science Library, Vol. 362, Nonlinear Cosmic Ray Diffusion Theories, ed. A. Shalchi (Berlin: Springer-Verlag), 362
Simpson, J. A., Anglin, J. D., Balogh, A., et al. 1992, A&AS, 92, 365
Smith, C. W., & Bieber, J. W. 1991, ApJ, 370, 435
Stone, E. C., Cummings, A. C., McDonald, F. B., et al. 2013, Sci, 341, 150
Strauss, R., & Potgieter, M. 2014a, SoPh, 289, 3197
Strauss, R., & Potgieter, M. 2014b, AdSpR, 53, 1015
Vos, E. E. 2016, PhD thesis, North-West University, Potchefstroom
Vos, E. E., & Potgieter, M. S. 2015, ApJ, 815, 119
Vos, E. E., & Potgieter, M. S. 2016, SoPh, 291, 2181
Webber, W. R., & Potgieter, M. S. 1989, ApJ, 344, 779